



A Journal of the Gesellschaft Deutscher Chemiker

Angewandte Chemie

GDCh

International Edition

www.angewandte.org

Accepted Article

Title: Semiconducting Polymer Dots with Dually Enhanced NIR-IIa Fluorescence for Through-Skull Mouse Brain Imaging

Authors: Zhe Zhang, Xiaofeng Fang, Zhihe Liu, Haichao Liu, Dandan Chen, Shuqing He, Jie Zheng, Bing Yang, Weiping Qin, Xuanjun Zhang, and Changfeng Wu

This manuscript has been accepted after peer review and appears as an Accepted Article online prior to editing, proofing, and formal publication of the final Version of Record (VoR). This work is currently citable by using the Digital Object Identifier (DOI) given below. The VoR will be published online in Early View as soon as possible and may be different to this Accepted Article as a result of editing. Readers should obtain the VoR from the journal website shown below when it is published to ensure accuracy of information. The authors are responsible for the content of this Accepted Article.

To be cited as: *Angew. Chem. Int. Ed.* 10.1002/anie.201914397
Angew. Chem. 10.1002/ange.201914397

Link to VoR: <http://dx.doi.org/10.1002/anie.201914397>
<http://dx.doi.org/10.1002/ange.201914397>

RESEARCH ARTICLE

Semiconducting Polymer Dots with Dually Enhanced NIR-IIa Fluorescence for Through-Skull Mouse Brain Imaging

Zhe Zhang,^[a, b] Xiaofeng Fang,^[a] Zhihe Liu,^[a] Haichao Liu,^[b] Dandan Chen,^[a] Shuqing He,^[a] Jie Zheng,^[b] Bing Yang,^[b] Weiping Qin,^[b] Xuanjun Zhang,^[c] Changfeng Wu^{*[a]}

Abstract: Fluorescence probes in NIR-IIa region (1300–1400 nm) show drastically improved imaging owing to the reduced photon scattering and autofluorescence in biological tissues. However, organic fluorophores in this region are largely unexplored. Here, we develop NIR-IIa polymer dots (Pdots) by a dual fluorescence enhancement mechanism. First, we used the aggregation induced emission of phenothiazine to reduce the nonradiative decay pathways of the polymers in condensed states. Second, we minimized the fluorescence quenching by different levels of steric hindrance to further boost the fluorescence. The resulting Pdots displayed a fluorescence QY of ~1.7% in aqueous solution, suggesting an enhancement of ~21 times in comparison with the original polymer in tetrahydrofuran (THF) solution. Small animal imaging by using the NIR-IIa Pdots exhibited a remarkable improvement in penetration depth and signal to background ratio, as confirmed by through-skull and through-scalp fluorescent imaging of the cerebral vasculature of live mice. This study indicates the promising potential of NIR-IIa Pdots for *in vivo* fluorescence imaging.

Introduction

Fluorescent probes play a versatile role in biological imaging and various bioassays. The development of *in vivo* fluorescence imaging has shown significant potential for a wide variety of molecular diagnostics and therapeutic applications.^[1] However, the majority of organic fluorophores show emissions in the visible region or the first near-infrared window (NIR-I, 700–900 nm), where the imaging suffers from substantial photon scattering and autofluorescence in biological tissues.^[2] Recent research efforts reveal a promising imaging window in the second near-infrared wavelength range (NIR-II, 1000–1700 nm), resulting in large penetration depth and high signal-to-noise ratio (SNR) for *in vivo* fluorescence imaging.^[3] Accordingly, NIR-II fluorescent probes have attracted considerable attention in the past few years.^[4] For

instance, Dai and coworkers developed a series of NIR-II fluorescent probes and demonstrated the superior performance of *in vivo* NIR-II imaging.^[5] Cheng et al. synthesized a diketopyrrolopyrrole polymer exhibiting NIR-II fluorescence, and the corresponding nanoparticles were capable of assisting accurate image-guided tumor surgery.^[6] Among those, the NIR-IIa (1300–1400 nm) window is particularly attractive because the reduced scattering and avoidance of water absorption above 1400 nm allow for through-skull fluorescence imaging of cerebral vasculature with unprecedented levels of penetration and resolution.^[7] However, organic fluorophores in this wavelength region have been scarcely explored so far.

Semiconducting polymer dots (Pdots) have demonstrated practical utilities in biological imaging and biosensing owing to their tunable optical properties.^[1a;1d;8] However, the semiconducting polymers in nanoparticle forms typically exhibit fluorescence quenching in comparison with the original polymers in organic solvents. The quenching can be attributed to intense inter- and intra-chain π - π stacking interactions, often resulting in the formation of non-emissive excimers and exciplexes.^[9] This phenomenon is known as the aggregation-caused quenching (ACQ) effect. In the visible wavelength region, fluorescence quenching in Pdots is moderate and can be comprised because they possess extremely large absorption coefficients and per-particle brightness is determined by the product of absorption cross section and fluorescence quantum yield (QY). Therefore, Pdots exhibit high brightness that is valuable for fluorescence imaging and biosensing applications.^[10] In many cases, the large absorption cross sections of Pdots are also favorable for photoacoustic imaging and photothermal therapy.^[11] However, semiconducting polymers are nearly non-fluorescent in the NIR-II region. The energy gap law predicts that the vibrational overlap between the ground and excited states largely determines the nonradiative decay rate.^[12] The nonradiative decay rate increases significantly with a decrease in the emission energy, making it difficult to obtain NIR-II fluorophores with a high QY. Energy migration in the large π -conjugated systems of semiconducting polymers may also lead to energy funneling to the non-emissive species, amplifying the fluorescence quenching effect. Therefore, the development of semiconducting polymers with strong fluorescence in the NIR-II region remains challenging.

Aggregation-induced emission (AIE) is a phenomenon wherein the fluorophore shows an emission boost when it transforms from an isolated molecule state to aggregated state.^[13] Mechanistic studies have suggested that, for an isolated AIE molecule in the excited state, energy is consumed by the free intramolecular motion, thereby quenching the emission.^[14] Such a nonradiative

[a] Dr. Z. Zhang, Dr. X. Fang, Dr. Z. Liu, Dr. D. Chen, Prof. S. He, Prof. C. Wu
Department of Biomedical Engineering, Southern University of Science and Technology, Shenzhen, Guangdong 518055 (China)
E-mail: wucf@sustech.edu.cn

[b] Dr. H. Liu, Prof. J. Zheng, Prof. B. Yang, Prof. W. Qin
State Key Laboratory of Integrated Optoelectronics, College of Electronic Science and Engineering, Jilin University, Changchun, Jilin 130012 (China)

[c] Prof. X. Zhang
Faculty of Health Science, University of Macau, Taipa, Macau SAR 999078 (China)

Supporting information for this article is given via a link at the end of the document.

RESEARCH ARTICLE

transition would be prevented in the aggregated state, wherein the free rotations are inhibited.^[9;15] Based on this mechanism, AIE molecules can be constructed by incorporating typical AIEgens, such as tetraphenylethene, hexaphenylsilole, and distyreneanthracene, into the molecular structure.^[16] The strong fluorescence intensity in the aggregated state and the variety of potential synthetic routes make AIE molecules one of the most important classes of fluorophores. The AIE fluorophores in nanoparticles provide promising platforms for fluorescence imaging.^[1a] Several reports have demonstrated the development of AIE nanoparticles for NIR-II imaging applications.^[17] Tang and coworkers developed short-wave infrared AIE dots, denoting real-time high-resolution imaging in live mice.^[18] However, fluorescent probes in the NIR-IIa window are still highly preferable owing to the superior imaging quality in this region.

Herein, we describe a molecular engineering strategy towards the development of semiconducting polymers in the NIR-II region. We designed nine polymers to propose a dual fluorescence enhancement mechanism to boost the NIR-II fluorescence of Pdots. On one hand, we use the AIE character of phenothiazine unit to reduce the nonradiative decay pathways of the polymer in aggregated states. On the other hand, we introduce bulky side-chain groups to weaken the intense inter- and intra-chain π - π stacking interactions via steric hindrance, further enhancing the fluorescence QY. Based on this dual enhancement strategy, the resulting NIR-II Pdots displayed a fluorescence QY of $\sim 1.7\%$ in aqueous solution, suggesting an enhancement of approximately 21 times in comparison with the original polymer in tetrahydrofuran (THF) solution. One of the resulting Pdots exhibits a fluorescence spectrum that strides the NIR-IIa region. Small animal imaging showed significant improvement in through-skull-scalp fluorescent imaging of the cerebral vasculature of live mice, indicating the promising potential of such a dual enhancement strategy for designing NIR-II fluorophores for *in vivo* fluorescence imaging.

Results and Discussion

We design the semiconducting polymers according to a classic donor-acceptor (D-A) structure. In D-A polymers, the highest occupied molecular orbital (HOMO) and the lowest unoccupied molecular orbital (LUMO) after orbital hybridization are mainly located at the donor and acceptor units, respectively.^[19] Therefore, a narrow bandgap between the HOMO and LUMO could be realized by using strong donor and acceptor units. The specific molecular engineering strategy is illustrated in Figure 1.

We choose phenothiazine as the donor because of several properties of this chromophore. First, the sulfur and nitrogen atoms endow phenothiazine with superior electron-donating ability, suggesting a suitable HOMO energy level. Second, the phenothiazine ring is an excellent nonplanar building block that can impede π -stacking aggregation and excimer formation in

conjugated polymers.^[20] Third, phenothiazine also possesses multiple reaction sites and excellent chemical reactivity, which facilitate the synthesis of the polymers and modification of the side-chain groups. More importantly, recent studies indicate that phenothiazine based small molecules show an apparent AIE feature.^[21] The heterocyclic ring in phenothiazine presents a dihedral angle of 153° because of the sp^3 -hybridized sulfur and nitrogen atoms.^[22] This geometric configuration guarantees the flexibility of the polymer, which implies that phenothiazine might induce AIE for the resulting polymers in aggregation state. Therefore, we attempt to use phenothiazine as the donor unit in the polymer synthesis to enhance the NIR-II fluorescence. Furthermore, benzothiazole and its derivatives (benzothiazole, BT; naphtho[2,3-c][1,2,5]thiadiazole, NT; and benzobisthiadiazole, BBTD) with different electron affinities were employed as acceptors to endow the polymers with highly shifted fluorescence wavelengths. Particularly, we anticipate to drive the fluorescence emission to the NIR-IIa window by using the extremely strong acceptor BBTD.

The large π -conjugated backbones of semiconducting polymers tend to have strong intermolecular interactions, inducing the formation of non-emissive excimers and exciplexes (ACQ phenomenon).^[9;23] It is worth noting that AIE and ACQ can exist simultaneously in one polymer owing to their different mechanisms. The intense intermolecular interactions may still attenuate the fluorescence in the aggregated state, even in AIE molecules. Therefore, the fluorescence intensity of AIE Pdots could be further improved by suppressing the ACQ effect in the semiconducting polymers. Toward this end, we introduce side groups on the nitrogen atoms of phenothiazine via nucleophilic substitution. The steric hindrance generated by the bulky side groups weakens the inter- and intra-chain interactions in the aggregated state, which is referred to as anti-ACQ. To examine the effectiveness of anti-ACQ, we choose three side groups that provided different levels of steric hindrance in polymer synthesis. Specifically, nine polymers were designed, namely P1a, P1b, P1c, P2a, P2b, P2c, P3a, P3b, and P3c, as shown in Figure S1. In the naming convention, the number 1, 2, or 3 distinguishes the main chain structures, whereas the letter a, b, or c represents the side chain groups.

Density functional theory calculations were first performed to predict the energy levels (Figure S14). The LUMOs were mainly distributed on the acceptors. As the electron affinity increased from P1c to P3c, the LUMO energy level decreased obviously. The combination of the lower LUMO energy level and constant HOMO energy level resulted in a narrow bandgap, suggesting a red-shift in the emission peak of the polymer. The HOMOs exhibited major delocalization on phenothiazine units with minimal overlap with the LUMOs, indicating typical intramolecular charge transfer within the polymer. All side chain groups exhibited almost no molecular orbital distribution, indicating that the side groups would not interfere with the fluorescence radiation transition.

RESEARCH ARTICLE

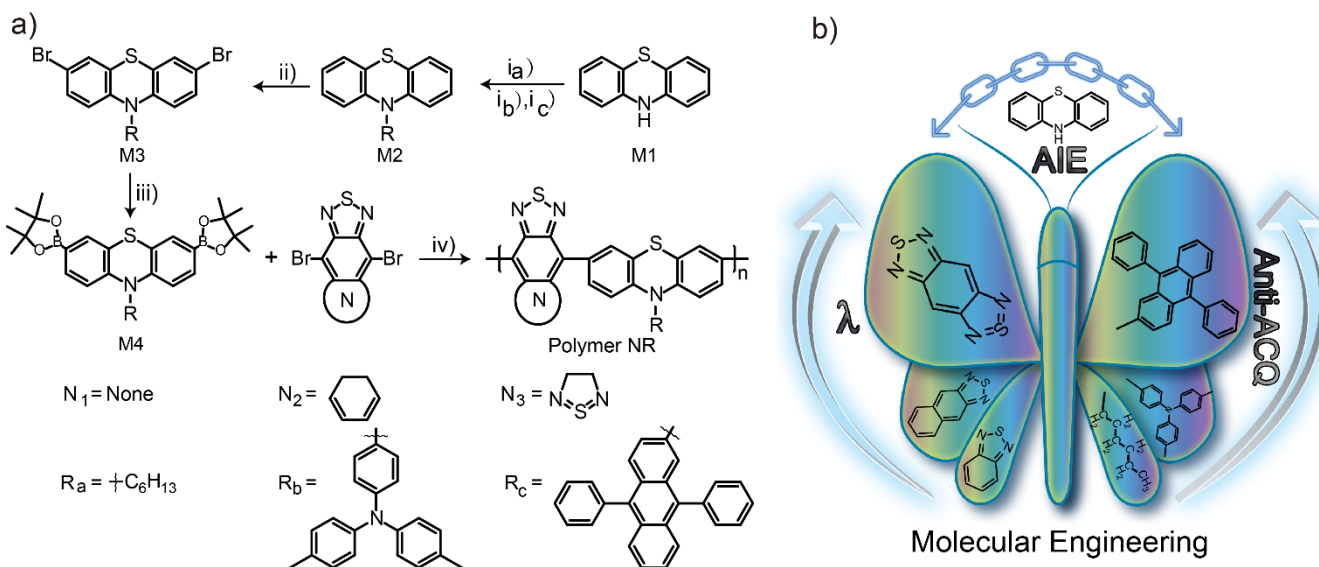


Figure 1. a) Synthetic route and conditions: i_a) DMSO/NaOH, 1-bromooctane, RT; i_b) 4-bromo-N,N-di-p-tolylaniline, HPTBu₃BF₄, NaOtBu, Pd₂(dba)₃, toluene, reflux; i_c) 2-bromo-9,10-diphenylanthracene, HPTBu₃BF₄, NaOtBu, Pd₂(dba)₃, toluene, reflux; ii) NBS, toluene, acetic acid, RT; iii) Bis(pinacolato)diboron, Pd(dppf)Cl₂, KOAc, dioxane, 80°C; and iv) Pd(PPh₃)₄, toluene, K₂CO₃, 85°C. b) Schematic of the general approach of molecular engineering for NIR fluorescence enhancement: i) acceptors with different electron affinities were employed to adjust the emission wavelength; ii) flexible phenothiazine enabled the generation of AIE character; and iii) fluorescence QY was further considerably improved by varying the side-chain groups. c) Spatial distributions of HOMO and LUMO along with their orbital energies for P1c, P2c, and P3c polymers.

Based on the molecular engineering strategy, the synthetic route was devised and implemented (Figure 1). The target side group was attached to phenothiazine via nucleophilic substitution (M2), and this intermediate product was brominated (M3) and boronized via Miyaura reaction (M4). Finally, M4 and brominated acceptors were polymerized by the Suzuki reaction. Detailed synthetic information and nuclear magnetic resonance spectroscopy data can be found in the Supporting Information. The number-average molecular weight (M_n) and polymer dispersity index (PDI) were evaluated by gel permeation chromatography, and the results are listed in Table 1.

The absorption and fluorescence spectra of the semiconducting polymers in organic solvent were investigated (Figure 2a). The emission of the polymers was successfully shifted from red (~600 nm) to NIR-II (~1300 nm) by varying the electron affinity of the acceptors. Polymers P3a, P3b, and P3c in THF exhibited two emission peaks at approximately 1130 and 1270 nm and absorption peak at approximately 740 nm (Figure S11). The fluorescence emission of P3c polymer strides the spectral range from 1000 to 1450 nm, indicating their great potential in NIR-IIa fluorescence imaging.

In our design, AIE is one of two key factors in realizing high fluorescence QY of the Pdots. To examine the AIE feature of the polymers, fluorescence images and spectra of the polymers in THF/water mixtures with different water volume fractions (f_w) were collected (Figure S13). In the fluorescence images, the solutions with higher f_w showed brighter signals (Figure 2b), indicating apparent AIE character. For a quantitative demonstration, the

ratio of the fluorescence peak intensity of the polymer in the THF/water mixture to that of the polymer in pure THF (I_{THF}/I_{0}) was calculated. As an example, for P3c, the fluorescence intensity decreased slightly when 10 vol% of water was added to the THF solution. This effect was attributed to the interaction between water and the polymers and the change of the hydrophobic environment. However, as f_w increased further, the fluorescence intensity increased continually until $f_w = 80$ vol%, revealing that the AIE signature prevails in the system.

Another key factor in dual fluorescence enhancement is the anti-ACQ effect. The fluorescence images of the three NIR-II polymers (P3a, P3b and P3c) and small dye molecule IR26 were collected in different states under the same imaging conditions (Figure 2c). The anti-ACQ effect was verified through the comparison of the samples from the same row in Figure 2c. By increasing the steric hindrance of side-chain groups, the mean fluorescence intensity was noticeably enhanced among the three polymers in the THF solution, whereas the AIE character was ineffective. Other effects of the side groups on the radiative transition could be excluded based on the results of the density functional theory calculations and the same backbones of the polymers possessing the similar spectra (e.g., P3a, P3b, and P3c). This anti-ACQ effect becomes even more pronounced in the Pdots forms because the bulky side group of P3c effectively prevents π -stacking aggregation and excimer/exciple formation in the Pdots with densely packed polymer chains (Figure 2d). As a further evidence, solid polymer powders demonstrated even brighter NIR-II fluorescence than the Pdots (Figure 2c), revealing great potential for applications requiring solid-state fluorescent

RESEARCH ARTICLE

materials. Again, P3c polymer powder exhibit stronger NIR-II fluorescence than P3a and P3b, further confirming the anti-ACQ effect by engineering the side chain groups.

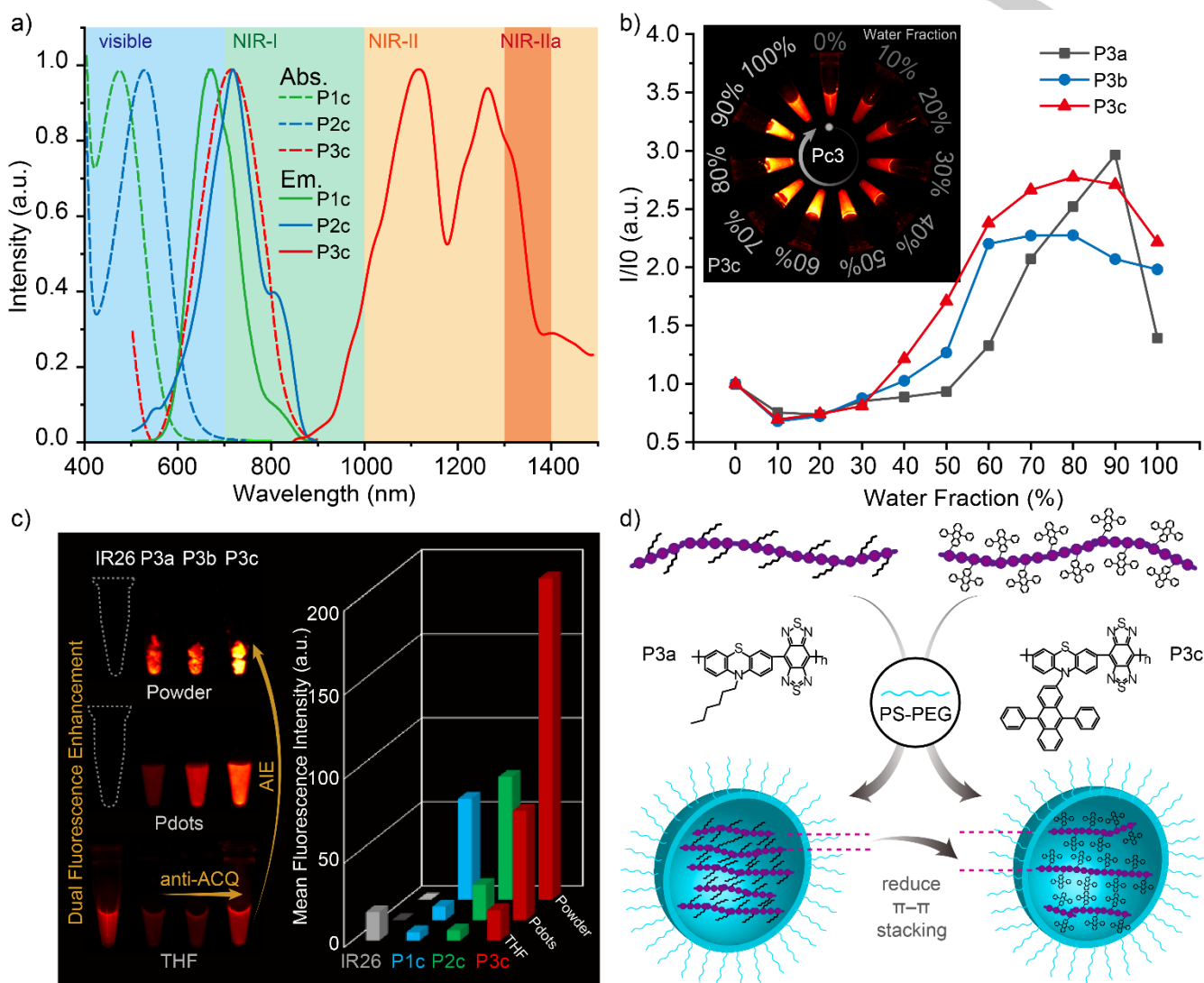


Figure 2. a) Absorption and fluorescence spectra of P1c, P2c, and P3c polymers in THF. b) Fluorescence intensity changes of P3a, P3b, and P3c in THF/water mixtures containing different water fractions. The 100% water fraction indicates the bare Pdots (without encapsulation) in water. I/I_0 is the ratio of the fluorescence peak intensity of the polymer in the THF/water mixture to that of the polymer in pure THF. The inset shows the fluorescence images of P3c in THF/water mixtures (100 $\mu\text{g}/\text{mL}$) containing different water fractions. The images were obtained using a 1250-nm long-pass filter under laser excitation at 808 nm (50 $\text{mW}\cdot\text{cm}^{-2}$). c) Fluorescence images of IR26 and Pdots in different states. Bottom row: IR26 in DCE and P3a, P3b, and P3c in THF (100 $\mu\text{g}/\text{mL}$); Middle row: Pdots of P3a, P3b, and P3c in water and IR26-doped polystyrene nanoparticles in water (100 $\mu\text{g}/\text{mL}$); Top row: IR26, P3a, P3b, and P3c powders. The images were recorded by using a 1250-nm long-pass filter under laser excitation at 808 nm (30 $\text{mW}\cdot\text{cm}^{-2}$). d) Schematic illustration of the formation of Pdots. A functional polymer PS-PEG was used for surface PEGylation that can increase blood circulation time for *in vivo* fluorescence imaging. The greater steric hindrance in P3c weakened the π - π stacking interaction, resulting in the anti-ACQ effect and a higher fluorescence QY.

Quantitative optical characterizations were performed to investigate the fluorescence dual enhancement in Pdots. The NIR-II fluorescence QYs were measured by using IR-26 in 1,2-dichloroethane (DCE) as a reference (QY = 0.5%).^[24] Table 1 shows the optical parameters of the semiconducting polymers and corresponding Pdots. Owing to the AIE character, all the QYs of Pdots are higher than that of the corresponding polymer in THF

solution, with most of them exhibiting a superior increase of approximately two times. In THF solution, the anti-ACQ effect of the side groups was not fully active because of the weak aggregation. In contrast, the tighter aggregation of Pdots accentuated the effect of fluorescence enhancement by the side-chain groups. The QYs of Pdots increased obviously from side group R_a to side group R_c, confirming the function of the side

RESEARCH ARTICLE

groups. Among the three side groups, diphenylanthracene significantly weakened the intermolecular interactions, resulting in the best anti-ACQ effect.

Table 1. Optical Properties of Semiconducting Polymers and the Resulting Pdots.

	$\lambda_{\text{abs}}^{\text{Pdots}}$ [nm] ^a	$\lambda_{\text{em}}(\Phi)^{\text{THF}}$ [nm, %] ^b	$\lambda_{\text{em}}(\Phi)^{\text{Pdots}}$ [nm, %]	$\Phi^{\text{Pdots}}/\Phi^{\text{THF}}$	E_g [eV] ^c	M_n [kDa] ^d	PDI ^e	Size [nm] ^f
P1a	456	674 (9)	699 (23)	2.6	1.53	5.0	3.21	16
P1b	509	649 (15)	687 (25)	1.7	1.53	6.3	3.11	18
P1c	482	669 (11)	685 (25)	2.3	1.55	4.4	4.17	18
P2a	537	683 (10)	740 (11)	1.1	1.36	4.4	1.57	14
P2b	522	659 (8)	732 (17)	2.1	1.46	4.5	1.55	16
P2c	538	717 (6)	731 (19)	3.2	1.46	5.2	2.58	17
P3a	736	1113, 1284 (0.08)	1090 (0.1)	1.3	0.90	3.2	3.51	24
P3b	759	1115, 1279 (0.3)	1088 (0.6)	2.0	0.89	4.9	1.56	14
P3c	746	1123, 1272 (0.6)	1083 (1.7)	2.2	0.89	2.8	1.68	16

a) Absorption maximum; b) emission maximum and fluorescence quantum efficiency; c) the optical bandgap was calculated from the intersection of the absorption and emission spectra; d) number-average molecular weight; e) polymer dispersity index; f) sizes of Pdots in water.

Based on this dual enhancement strategy, the P3c Pdots exhibited a NIR-II fluorescence QY of ~1.7% in aqueous solution, corresponding to an enhancement of approximately 21 times as compared to P3a in THF. It represents the highest QY reported so far for NIR-II Pdots. It is worth noting that the brightness of the fluorescent probes is determined by the product of absorption cross section and fluorescence quantum yield.^[1d] UV-Vis-NIR absorption measurements were performed for P3c Pdots, IR26, and Indocyanine Green (ICG) to compare their brightness. The results indicated that the peak absorption cross section of P3c Pdots (~16-nm-diameter) at 746 nm was ~180 times larger than that of IR26 at 935 nm, and ~60 times higher than that of ICG at 780 nm, respectively. Considering the same excitation wavelength at 808 nm, the absorption cross section of P3c Pdots (~16 nm) was ~190 times higher than that of IR26, and ~100 times higher than that of ICG, respectively. Combined with the QY values, the NIR-II fluorescence brightness of single P3c Pdot is over 500 times higher than single dye fluorophores. We also compared the fluorescence brightness of the three probes at the same weight concentration in solutions under 808 nm excitation. As indicated in Figure S16, the P3c Pdots in water is ~2 times brighter than IR26 in DMSO and ~15 times brighter than ICG in water for the emission collected by a 1250 nm long-pass filter. Based on these results, the Pdots outperform the fluorescent dyes at both single probe level and bulk solutions.

The particle size, morphology, photostability, and biocompatibility of the Pdots were further characterized to evaluate their application potential. P3c Pdots was selected for further investigations based on their outstanding fluorescence QYs. The fluorescence spectrum of the P3c Pdots in aqueous solution was somewhat different from that of P3c in THF because of aggregated conformation (Figure 3a). Still, the emission profile strides the broad wavelength range from 1000 to 1400 nm. The emission intensity in the NIR-IIa region was relatively decreased as compared to that of the polymer in THF solution (Figure 2a). Dynamic light scattering demonstrated that the Pdots were well dispersed in water with an average hydrodynamic diameter of ~16 nm. Transmission electron microscopy (TEM) imaging indicated the spherical morphologies of the well-dispersed nanoparticles (Figure 3b). Photostability was examined by monitoring the fluorescence intensity under continuous laser illumination (808 nm, 1.0 W/cm²). The fluorescence of the P3c Pdots remained nearly 70% of the original intensity after 120 min of laser exposure, while the IR26 and ICG dyes were completely photobleached in 10 min (Figure 3c). This comparison clearly indicated the superior photostability of Pdots as compared to the small dye molecules. Biocompatibility is a vital consideration for biological applications. As shown in Figure 3d, the Pdots showed low cytotoxicity, even at high concentrations (100 µg/mL), indicating their biocompatible feature. Collectively, these results indicate that the P3c-Pdots are an excellent NIR-II fluorophore for bioimaging.

RESEARCH ARTICLE

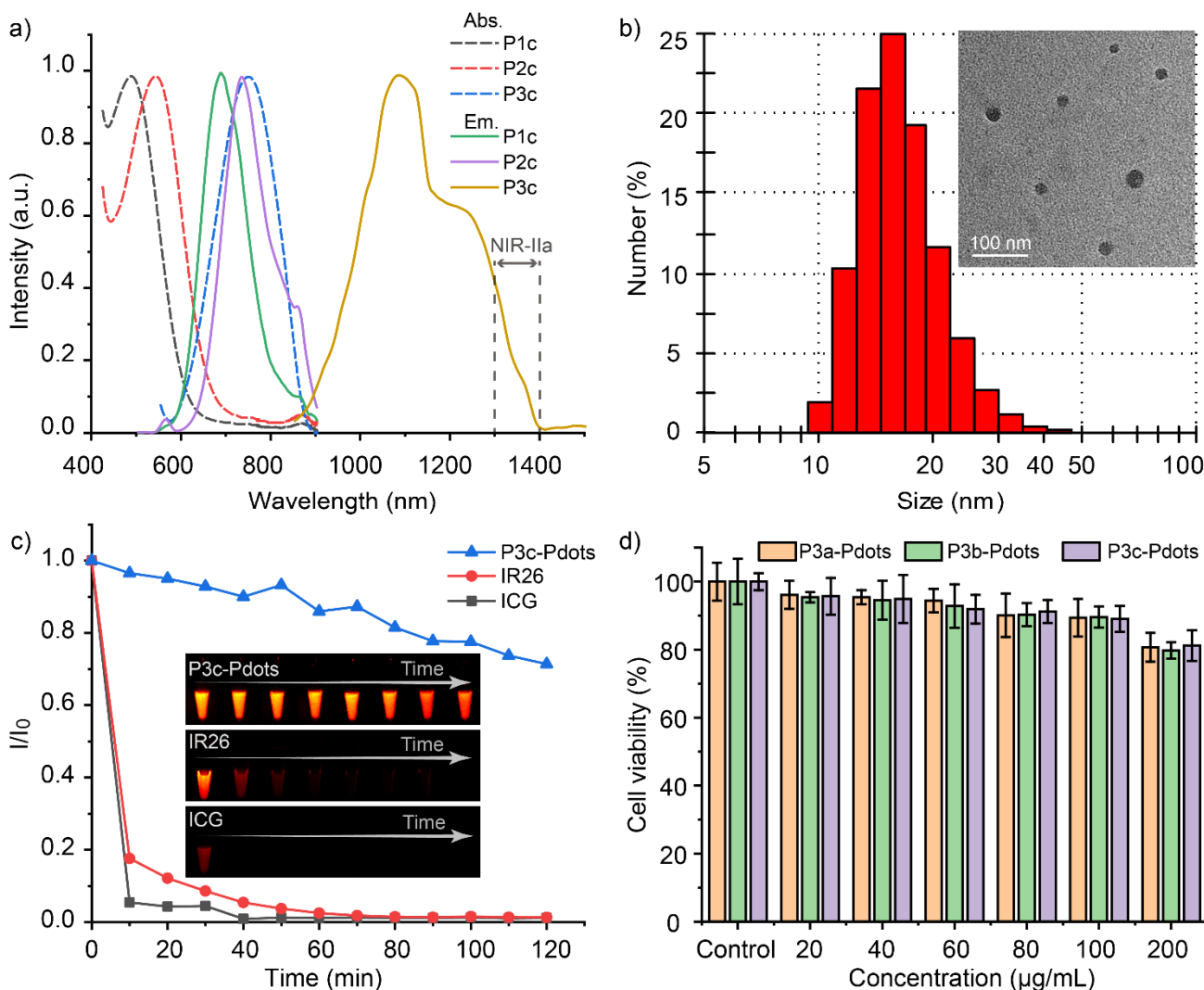


Figure 3. a) Absorption and fluorescence spectra of P1c, P2c and P3c Pdots in water. b) Distribution of hydrodynamic diameter of the P3c Pdots determined by dynamic light scattering. The inset shows a representative TEM image of the P3c Pdots. c) Photostability of bare P3c-Pdots (without encapsulation) in water, ICG in water, and IR26 in dimethyl sulfoxide under continuous 808 nm radiation (1.0 W/cm^2). I/I_0 is the ratio of the mean fluorescence intensity of the samples after radiation to that of the original mean fluorescence intensity. The inset shows the corresponding fluorescence images, using a 1250-nm long-pass filter under laser excitation at 808 nm ($30 \text{ mW}\cdot\text{cm}^{-2}$). d) Results of a cellular toxicity study in which HeLa cells were incubated with different concentrations of Pdots.

Optical imaging of the brain in the traditional wavelength region (400–900 nm) is severely constrained by the light penetration depth in biological tissues.^[3,25] Recent studies have demonstrated that fluorescence collection in the 1.3–1.4 μm NIR-IIa window led to drastically improved imaging of mouse cerebral vasculature because of the minimal scattering by rejecting photons wavelengths shorter than 1.3 μm while avoiding an increase in light absorption from water vibrational overtone modes above $\sim 1.4 \mu\text{m}$.^[7] We performed *in vivo* non-invasive fluorescence imaging of live mouse brain with the PEGylated P3c Pdots. A solution of the Pdots was injected into a mouse via the tail vein, and the head of the mouse with intact skull and scalp (hair shaved off only) was imaged by a small animal imaging setup. Low excitation power density ($70 \text{ mW}\cdot\text{cm}^{-2}$, 808 nm) was used to minimize damage to the mouse while maintaining image quality.

Broad NIR-II emission spectrum of the P3c Pdots gives multiple choices on the fluorescence acquisition range. Despite the relatively small emission profile of Pdots beyond 1300 nm, fluorescence imaging by a 1319 nm long-pass filter produces much sharper image than that by a 1250 nm long-pass filter (Figure 4a). The comparison of intensity profiles of cerebral vessels collected by the two filters confirms the high signal to background ratio (SBR) in the NIR-IIa region (Figure 4b, 5c). The P3c Pdots allowed clear visualization of the cerebrovascular structures under the intact skull and scalp (Figure 4a), indicating the large penetration depth enabled by the unique NIR-IIa emission. Thanks to the distinct fluorescence of Pdots and low autofluorescence in this region, high-quality imaging yielded well-resolved distance between cerebral blood vessels (Figure 4c). As seen from time-lapse imaging, the high SBR remains relatively

RESEARCH ARTICLE

constant in 180 min because of the relatively long circulation half-life (~6.6 hours) of the PEGylated Pdots (Figure S17). In contrast,

small molecule dyes such as ICG was usually cleared in ~5 minutes,^[26] which led to a very short imaging window.

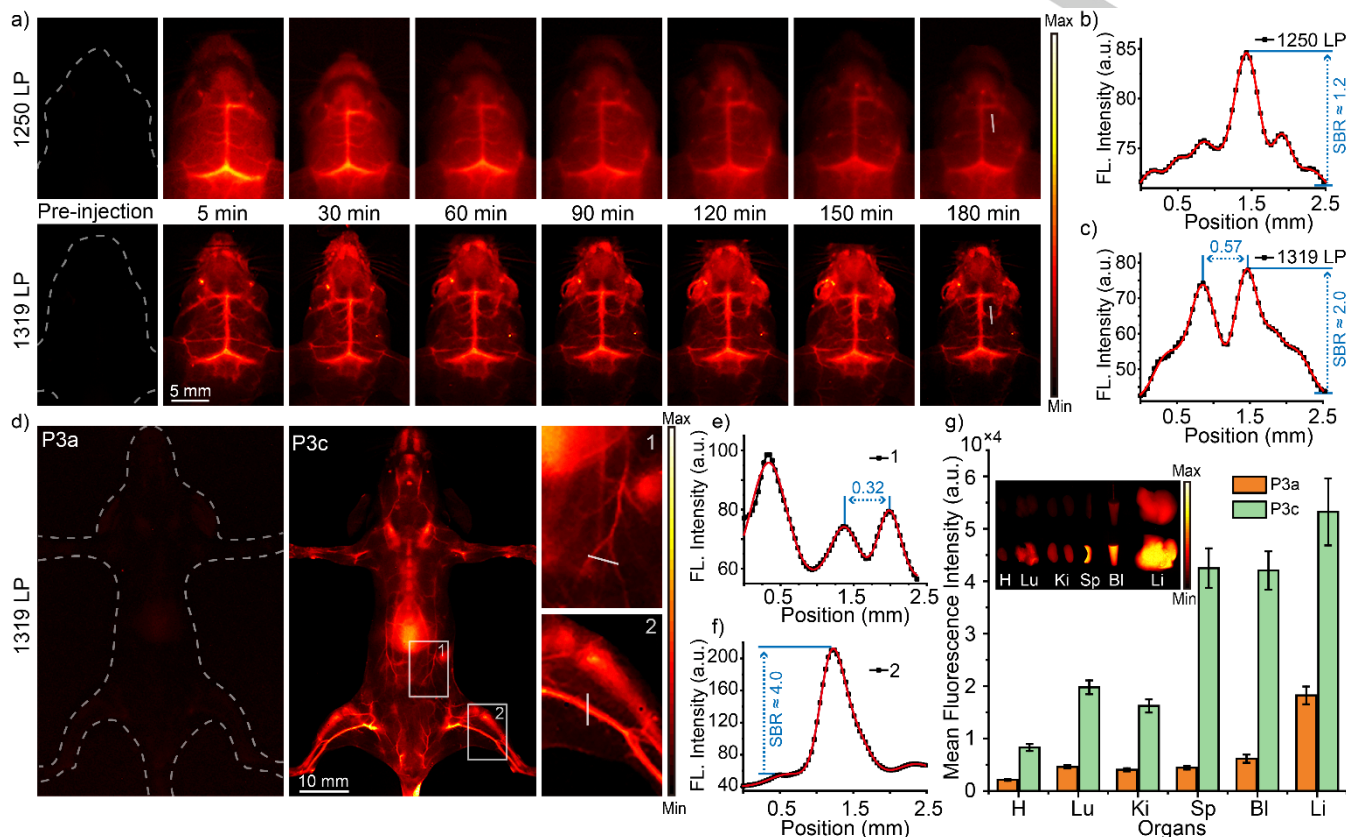


Figure 4. a) *In vivo* NIR-II fluorescence imaging of mouse brain at designated time points after intravenous injection of P3c Pdots (100 μ L, 1 mg/mL). The top panel shows the images collected by a 1250 nm long-pass filter, while the bottom shows those collected by a 1319 nm long-pass filter. b) Cross-sectional intensity profile along the white line in images collected by a 1250 nm long-pass filter with the peak fitted to a Gaussian function (red curve). c) Cross-sectional intensity profile along the white line in images collected by a 1319 nm long-pass filter with the peak fitted to a Gaussian function (red curve). d) *In vivo* NIR-II fluorescence images of mouse hindlimb vasculature 5 min after intravenous injection of P3a Pdots (100 μ L, 1 mg/mL) and P3c Pdots (100 μ L, 1 mg/mL), respectively. e) Cross-sectional intensity profile along the white line in c) #1 with the peak fitted to a Gaussian function (red curve). f) Cross-sectional intensity profile along the white line in c) #2 with the peak fitted to a Gaussian function (red curve). g) Mean fluorescence intensity of the heart (H), lung (Lu), kidney (Ki), spleen (Sp), blood (Bl), and liver (Li) at 24 h after the injection of the P3a and P3c Pdots, respectively. The inset shows the fluorescence images of the heart, lung, kidney, spleen, blood, and liver of the injected mouse. The images in d) and g) were obtained using a 1319-nm long-pass filter under 808-nm laser excitation (70 mW \cdot cm⁻²).

Whole-body NIR-IIa fluorescence imaging was finally performed to reaffirm the superior performance of the Pdots achieved by molecular engineering. P3a and P3c Pdots were used for whole-body imaging and compared under the same conditions. In the image obtained using P3a Pdots, the mouse body was nearly invisible (Figure 4d). In contrast, the P3c Pdots with AIE and stronger anti-ACQ effects resulted in much higher SBR and more details were achieved from the image (Figure 4e, 5f). This comparative imaging clearly demonstrated the improvement provided by the P3c Pdots with respect to the P3a Pdots, revealing the successful dual fluorescence enhancement based on the AIE and anti-ACQ effects. The major organs were dissected from the mouse 24 h after injection and quantitatively analyzed by fluorescence imaging (Figure 4g). The analysis results indicated that the Pdots were mainly distributed in the liver, blood, and spleen. The *in vivo* imaging results reveal that the

unique optical properties of P3c Pdots are promising NIR-IIa fluorophore for small animal studies.

Conclusion

In summary, a molecular engineering strategy was proposed to identify new NIR-II fluorophores for bioimaging. Specifically, nine semiconducting polymers were designed and synthesized to validate a dual fluorescence enhancement mechanism. The adjustment of electron affinity realized tunable excitation and emission wavelengths, with emission in the range of 600–1400 nm. The donor unit phenothiazine endowed the polymers with a narrow bandgap along with AIE character, leading to strong emission in the corresponding Pdots. Side groups provided different levels of steric hindrance to weaken the intermolecular

RESEARCH ARTICLE

interactions. This anti-ACQ effect further improved the fluorescence QY based on the AIE character. Under the dual enhancement by AIE character and anti-ACQ effect, the NIR-II fluorescence QY of P3c Pdots was approximately 21 times higher than that of P3a in THF. We used the P3c Pdots for *in vivo* NIR-II fluorescence imaging of mouse brain. Because the unique emission strides the NIR-IIa region, the through-scalp and through-skull imaging show clear visualization of cerebral vasculature. This study reveals the great potential of dual fluorescence enhancement based on the AIE and anti-ACQ effects for obtaining superior NIR-II fluorophores.

Acknowledgements

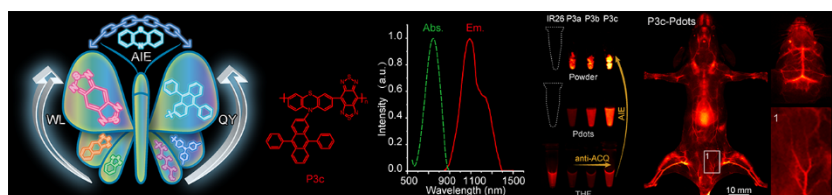
C. Wu acknowledges financial support from the National Natural Science Foundation of China (NSFC) (81771930) and Shenzhen Science and Technology Innovation Commission (JCYJ20170307110157501). The authors declare no competing financial interest.

Keywords: molecular engineering • NIR-II fluorescence imaging • semiconducting polymers • aggregation-induced emission • polymer dots

- [1] a) H.-S. Peng, D. T. Chiu, *Chem. Soc. Rev.* **2015**, *44*, 4699-4722; b) J. N. Liu, W. Bu, J. Shi, *Chem. Rev.* **2017**, *117*, 6160-6224; c) L. Yan, K. Pu, *Adv. Sci.* **2017**, *4*, 1600481; d) C. Wu, D. T. Chiu, *Angew. Chem. Int. Ed.* **2013**, *52*, 3086-3109.
- [2] a) G. Hong, S. Diao, A. L. Antaris, H. Dai, *Chem. Rev.* **2015**, *115*, 10816-10906; b) J. Huang, C. Xie, X. Zhang, Y. Jiang, J. Li, Q. Fan, K. Pu, *Angew. Chem. Int. Ed.* **2019**, *58*, 15120-15127.
- [3] G. Hong, A. L. Antaris, H. Dai, *Nat. Biomed. Eng.* **2017**, *1*, 0010.
- [4] a) Y. Cai, Z. Wei, C. Song, C. Tang, W. Han, X. Dong, *Chem. Soc. Rev.* **2019**, *48*, 22-37; b) C. Li, Q. Wang, *ACS nano* **2018**, *12*, 9654-9659; c) Y. Tang, Y. Li, X. Lu, X. Hu, H. Zhao, W. Hu, F. Lu, Q. Fan, W. Huang, *Adv. Funct. Mater.* **2019**, *29*, 1807376.
- [5] a) G. Hong, Y. Zou, A. L. Antaris, S. Diao, D. Wu, K. Cheng, X. Zhang, C. Chen, B. Liu, Y. He, J. Z. Wu, J. Yuan, B. Zhang, Z. Tao, C. Fukunaga, H. Dai, *Nat. Commun.* **2014**, *5*, 4206; b) Q. Yang, Z. Hu, S. Zhu, R. Ma, H. Ma, Z. Ma, H. Wan, T. Zhu, Z. Jiang, W. Liu, L. Jiao, H. Sun, Y. Liang, H. Dai, *J. Am. Chem. Soc.* **2018**, *140*, 1715-1724; c) S. Zhu, S. Herraiz, J. Yue, M. Zhang, H. Wan, Q. Yang, Z. Ma, Y. Wang, J. He, A. L. Antaris, Y. Zhong, S. Diao, Y. Feng, Y. Zhou, K. Yu, G. Hong, Y. Liang, A. J. Hsueh, H. Dai, *Adv. Mater.* **2018**, *30*, e1705799.
- [6] K. Shou, Y. Tang, H. Chen, S. Chen, L. Zhang, A. Zhang, Q. Fan, A. Yu, Z. Cheng, *Chem. Sci.* **2018**, *9*, 3105-3110.
- [7] G. Hong, S. Diao, J. Chang, A. L. Antaris, C. Chen, B. Zhang, S. Zhao, D. N. Atochin, P. L. Huang, K. I. Andreasson, C. J. Kuo, H. Dai, *Nat. Photonics* **2014**, *8*, 723-730.
- [8] a) J. Li, J. Rao, K. Pu, *Biomater.* **2018**, *155*, 217-235; b) L. Feng, C. Zhu, H. Yuan, L. Liu, F. Lv, S. Wang, *Chem. Soc. Rev.* **2013**, *42*, 6620-6633; c) Y. Jiang, J. McNeill, *Chem. Rev.* **2017**, *117*, 838-859; d) Y. Jiang, M. Novoa, T. Nongnual, R. Powell, T. Bruce, J. McNeill, *Nano Lett.* **2017**, *17*, 3896-3901.
- [9] Y. Hong, J. W. Lam, B. Z. Tang, *Chem. Commun.* **2009**, *40*, 4332-4353.
- [10] a) C. Wu, C. Szymanski, Z. Cain, J. McNeill, *J. Am. Chem. Soc.* **2007**, *129*, 12904-12905; b) C. Wu, C. Szymanski, J. McNeill, *Langmuir* **2006**, *22*, 2956-2960; c) X. Chen, Z. Liu, R. Li, C. Shan, Z. Zeng, B. Xue, W. Yuan, C. Mo, P. Xi, C. Wu, Y. Sun, *ACS nano* **2017**, *11*, 8084-8091; d) K. Y. Pu, B. Liu, *Biosens Bioelectron* **2009**, *24*, 1067-1073; e) J. Lin, X. Zeng, Y. Xiao, L. Tang, J. Nong, Y. Liu, H. Zhou, B. Ding, F. Xu, H. Tong, Z. Deng, X. Hong, *Chem. Sci.* **2019**, *10*, 1219-1226; f) X. Lu, P. Yuan, W. Zhang, Q. Wu, X. Wang, M. Zhao, P. Sun, W. Huang, Q. Fan, *Polym. Chem.* **2018**, *9*, 3118-3126.
- [11] a) K. Pu, S. Adam, J. J. Jesse, V. J. Mei, G. Sanjiv, S. Z. Bao, J. Rao, *Nature Nanotech.* **2014**, *9*, 233-239; b) Z. Wang, X. Zhen, P. K. Uppaturi, Y. Jiang, J. Lau, M. Pramanik, K. Pu, B. Xing, *ACS nano* **2019**, *13*, 5816-5825.
- [12] R. Englman, J. Jortner, *Mol. Phys.* **1970**, *18*, 145-164.
- [13] J. Luo, Z. Xie, J. W. Y. Lam, L. Cheng, H. Chen, C. Qiu, H. S. Kwok, X. Zhan, Y. Liu, D. Zhu, B. Z. Tang, *Chem. Commun.* **2001**, 1740-1741.
- [14] a) E. P. J. Parrott, N. Y. Tan, R. Hu, J. A. Zeidler, B. Z. Tang, E. Pickwell-MacPherson, *Mater. Horiz.* **2014**, *1*, 251-258; b) G. Yu, S. Yin, Y. Liu, J. Chen, X. Xu, X. Sun, D. Ma, X. Zhan, Q. Peng, Z. Shuai, B. Tang, D. Zhu, W. Fang, Y. Luo, *J. Am. Chem. Soc.* **2005**, *127*, 6335-6346; c) Q. Peng, Y. Yi, Z. Shuai, J. Shao, *J. Am. Chem. Soc.* **2007**, *129*, 9333-9339.
- [15] a) F. Bu, R. Duan, Y. Xie, Y. Yi, Q. Peng, R. Hu, A. Qin, Z. Zhao, B. Z. Tang, *Angew. Chem. Int. Ed.* **2016**, *127*, 14700-14705; b) N. L. C. Leung, X. Ni, Y. Wangzhang, L. Yang, W. Qunyan, P. Qian, M. Qian, J. W. Y. Lam, T. Ben Zhong, *Chem.* **2015**, *20*, 15349-15353; c) J. Chen, C. C. W. Law, J. W. Y. Lam, Y. Dong, S. M. F. Lo, I. D. Williams, D. Zhu, B. Z. Tang, *Chem. Mater.* **2003**, *15*, 1535-1546.
- [16] a) R. Hu, N. L. C. Leung, B. Z. Tang, *Chem. Soc. Rev.* **2014**, *43*, 4494-4562; b) S. Xu, Y. Duan, B. Liu, *Adv. Mater.*, *0*, 1903530.
- [17] a) Z. Sheng, B. Guo, D. Hu, S. Xu, W. Wu, W. H. Liew, K. Yao, J. Jiang, C. Liu, H. Zheng, *Adv. Mater.* **2018**, 1800766; b) J. Qi, C. Sun, A. Zebibula, H. Zhang, R. T. K. Kwok, X. Zhao, W. Xi, J. W. Y. Lam, J. Qian, B. Z. Tang, *Adv. Mater.* **2018**, *30*, e1706856; c) N. Alifu, A. Zebibula, J. Qi, H. Zhang, C. Sun, X. Yu, D. Xue, J. W. Y. Lam, G. Li, J. Qian, B. Z. Tang, *ACS nano* **2018**, *12*, 11282-11293.
- [18] W. Chen, C. A. Cheng, E. D. Cosco, S. Ramakrishnan, J. G. P. Lingg, O. T. Bruns, J. I. Zink, E. M. Sletten, *J. Am. Chem. Soc.* **2019**, *141*, 12475-12480.
- [19] Z. G. Zhang, J. Wang, *J. Mater. Chem.* **2012**, *22*, 4178-4187.
- [20] A. C. B. Rodrigues, J. Pina, W. Dong, M. Forster, U. Scherf, J. S. Seixas de Melo, *Macromol.* **2018**, *51*, 8501-8512.
- [21] X. Jiang, H. Gao, X. Zhang, J. Pang, Y. Li, K. Li, Y. Wu, S. Li, J. Zhu, Y. Wei, L. Jiang, *Nat. Commun.* **2018**, *9*, 3799.
- [22] A. P. Kulkarni, Y. Zhu, A. Babel, P. T. Wu, S. A. Jenekhe, *Chem. Mater.* **2008**, *20*, 4212-4223.
- [23] a) X. Cai, A. Bandla, D. Mao, G. Feng, W. Qin, L. D. Liao, N. Thakor, B. Z. Tang, B. Liu, *Adv. Mater.* **2016**, *28*, 8760-8765; b) J. Mei, N. L. Leung, R. T. Kwok, J. W. Lam, B. Z. Tang, *Chem. Rev.* **2015**, *115*, 11718-11940.
- [24] a) J. Cornil, I. Gueli, A. Dkhissi, J. C. Sancho-Garcia, E. Hennebicq, J. P. Calbert, V. Lemaire, D. Beljonne, J. L. Brédas, *J. Chem. Phys.* **2003**, *118*, 6615-6623; b) J. E. Murphy, M. C. Beard, A. G. Norman, A. S. Phillip, J. C. Johnson, Y. Pingrong, O. I. Micić, R. J. Ellingson, A. J. Nozik, *J. Amer. Chem. Soc.* **2006**, *128*, 3241-3247.
- [25] S. Diao, J. L. Blackburn, G. Hong, A. L. Antaris, J. Chang, J. Z. Wu, B. Zhang, K. Cheng, C. J. Kuo, H. Dai, *Angew. Chem. Int. Ed.* **2015**, *54*, 14758-14762.
- [26] C. Li, Y. Zhang, M. Wang, Y. Zhang, G. Chen, L. Li, D. Wu, Q. Wang, *Biomater.* **2014**, *35*, 393-400.

RESEARCH ARTICLE

RESEARCH ARTICLE



We demonstrate a molecular engineering strategy to enhance NIR-IIa fluorescence of polymer dots by managing the aggregation-induced emission (AIE) and aggregation-caused quenching (ACQ) effects. The polymer dots enabled a remarkable improvement in penetration depth and signal to background ratio in through-skull and through-scalp fluorescent imaging of the cerebral vasculature of live mice.

Authors: Zhe Zhang, Xiaofeng Fang, Zhihe Liu, Haichao Liu, Dandan Chen, Shuqing He, Jie Zheng, Bin Yang, Weiping Qin, Xuanjun Zhang, Changfeng Wu

Corresponding Author*: Changfeng Wu

E-mail address: wucf@sustech.edu.cn

Page No.–Page No.